Chinese Chemical Letters 33 (2022) 2911–2914

Contents lists available at ScienceDirect

Chinese Chemical Letters

journal homepage: www.elsevier.com/locate/cclet

Tailoring the surface structure of iron compounds to optimize the selectivity of 3-nitrostyrene hydrogenation reaction over Pt catalyst

Ying Zhang[a,b,1], Tongtong Gao[b,c,1], Chengshan Dai[b,d], Liyun Zhang[e], Yiming Niu[b,d], Junnan Chen[b,d], Zhong-Wen Liu[c,**], Bingsen Zhang[b,d,*]

[a] School of Petrochemical Engineering, Liaoning Shihua University, Fushun 113001, China
[b] Shenyang National Laboratory for Materials Science, Institute of Metal Research, Chinese Academy of Sciences, Shenyang 110016, China
[c] Key Laboratory of Syngas Conversion of Shaanxi Province, School of Chemistry and Chemical Engineering Shaanxi Normal University, Xi'an 710119, China
[d] School of Materials Science and Engineering, University of Science and Technology of China, Shenyang 110016, China
[e] Department of Chemical Engineering, Qufu Normal University, Qufu 273165, China

ARTICLE INFO

Article history:
Received 26 July 2021
Revised 17 September 2021
Accepted 18 October 2021
Available online 23 October 2021

Keywords:
Pt
Electronic structure
Surface structure
Iron compounds
Selective hydrogenation
3-Nitrostyrene

ABSTRACT

Selective hydrogenation of substituted nitroarenes is an important reaction to obtain amines. Supported metal catalysts are wildly used in this reaction because the surface structure of supports can tune the properties of the supported metal nanoparticles (NPs) and promote the selectivity to amines. Herein, Pt NPs were immobilized on FeOOH, Fe_3O_4 and α-Fe_2O_3 nanorods to synthesize a series of iron compounds supported Pt catalysts by liquid phase reduction method. Chemoselective hydrogenation of 3-nitrostyrene to 3-aminostyrene was used as probe reaction to evaluate the performance of the catalysts. The results show that Pt/FeOOH exhibits the highest selectivity and activity. FeOOH support with pores and -OH groups can tune the electronic structure of Pt NPs. The positive charge of Pt NPs supported on FeOOH is key factor for improving the catalytic performance.

Selective hydrogenation of aryl nitro compounds to amines is an essential step to obtain intermediate product for fine chemicals, including pharmaceuticals, herbicides, perfumes and dyes [1-3]. The challenge for this reaction is the hydrogenation of nitro group when another reducible group (C=C, C=O and –X, *etc.*) simultaneously present in one molecule, because most transition metal catalysts cannot distinguish nitro from reducible groups for selective hydrogenation. Over the last few decades, many efforts have been made to synthesize highly selectivity and activity catalysts for the preferential adsorption of nitro group in the presence of one or more reducible groups [4–7]. For example, some metal catalysts (*e.g.*, Au, Pd and Ag) were found to present high chemoselectivity for the hydrogenation of nitrostyrene (NS) to aminostyren (AS) [8,9]. However, due to their intrinsically low capability to activate H_2 molecule, these catalysts usually exhibited at least one order of magnitude less active than that of Pt metal catalysts [10,11]. Pt-based catalysts are the most widely used in this reaction because they exhibited high activity in the hydrogenation of NS, but it gave a low selectivity to AS since Pt was more effective for carbon–carbon covalent bond in the reduction of NS. To enhance the selectivity of AS over Pt catalysts, the researchers developed some strategies, such as introducing a modifier to the reaction [12], adding a second metal to Pt [5,13], and choosing appropriate reducible oxides as supports [14,15]. Since the supports are not inert and the interaction with nanoparticles (NPs) gives to new interface phenomena, the immobilized NPs on supports is considered as an efficient approach to enhance the stability and control spatial distribution of metal NPs [16,17]. Furthermore, the interaction between metal NPs and support may tune the electronic properties of Pt, which play a crucial role in determining the adsorption behavior of functional groups and the dissociation behavior of H_2 [18]. For instance, the hydrogenation performance of substituted nitroarenes over FeO_x-supported Pt single-atom and pseudo-single-atom catalysts were investigated, illustrating that significant electron transfers from the Pt atoms or ensembles to the FeO_x support, which was beneficial to improve the selective hydrogenation of NS to AS [11]. Iron compounds are widely used as metal oxide support due to their excellent performance, structure, surface properties and abundance [19–23].

* Corresponding authors at: Shenyang National Laboratory for Materials Science, Institute of Metal Research, Chinese Academy of Sciences, Shenyang 110016, China.
** Corresponding author.
E-mail addresses: bszhang@imr.ac.cn (B. Zhang), zwliu@snnu.edu.cn (Z.-W. Liu).
[1] These authors contributed equally to this work.

https://doi.org/10.1016/j.cclet.2021.10.049
1001-8417/

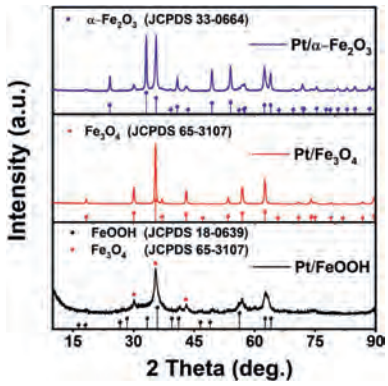

Fig. 1. XRD patterns of Pt/FeOOH, Pt/Fe_3O_4 and Pt/α-Fe_2O_3 catalysts.

Herein, the influence of iron compounds surface structure on catalytic performances of Pt NPs was studied and correlated to the activity/selectivity of the chemoselective hydrogenation of 3-NS. Three kinds of iron compounds FeOOH, Fe_3O_4 and α-Fe_2O_3 nanaorods were firstly synthesized. Then, Pt NPs supported on these three iron compounds were prepared by ethylene glycol (EG) reduction method [24,25]. Advanced characterization and analysis were performed to explore the interaction between Pt NPs and their supporting matrix.

The morphology and structure of the iron compounds were firstly studied. Fig. S1 (Supporting information) shows the optical digital images of the iron compound supports. The color of FeOOH, Fe_3O_4 and α-Fe_2O_3 powders are dark-red, black and red, respectively. Fig. S2 (Supporting information) displays the low-magnification transmission electron microscopy (TEM) and high-resolution TEM (HRTEM) images of the iron compounds. It is clearly that all the supports have similar rod-like architectures. Interestingly, there are many mesopores on the surface of FeOOH, which could be act as the anchor sites for metal active components. HRTEM observations further identified the crystallographic properties of the iron compound supports. The interplanar spacing (d) of lattice fringes are coincide with (400) and ($\bar{2}11$) planes of FeOOH, (111) and ($3\bar{1}1$) planes of Fe_3O_4 and (104) and ($1\bar{2}0$) planes of α-Fe_2O_3, respectively. The X-ray diffraction (XRD) patterns Fig. S3 in Supporting information further illustrate the main phase structure can be attributed to orthorhombic FeOOH (JCPDS No. 18-0639), cubic Fe_3O_4 (JCPDS No. 65-3107) and hexagonal α-Fe_2O_3 (JCPDS No. 33-0664) phases, respectively. The nitrogen adsorption–desorption isotherms were also obtained, as shown in Fig. S4 (Supporting information). It can be seen that FeOOH display obvious mesoporous structure. The measured Brunner-Emmet-Teller (BET) surface areas of FeOOH, Fe_3O_4 and α-Fe_2O_3 were 104.0, 24.4 and 24.5 cm^2/g, respectively. Compared with Fe_3O_4 and α-Fe_2O_3, the larger BET surface area of FeOOH could be ascribed to the formation of hollow pore structure of the FeOOH support, which is observed from the TEM images. Fig. S5 (Supporting information) shows the X-ray photoelectron spectra (XPS) survey spectra and N 1s spectra of FeOOH, Fe_3O_4 and α-Fe_2O_3 supports. No N peaks were observed in full scan survey, indicating that there is no residual N element in FeOOH, Fe_3O_4 and α-Fe_2O_3 supports during the synthesis process.

The crystal structures of Pt/FeOOH, Pt/Fe_3O_4 and Pt/α-Fe_2O_3 samples are analyzed by XRD patterns and HRTEM images. The main diffraction peaks in Fig. 1 are assigned to the corresponding supports. For FeOOH support in Pt/FeOOH catalyst, the XRD pattern is slightly different with standard JCPDS No. 18-0639. The diffraction peaks located at $2\theta = 30.1°$ and 43.1° and the overlap peak at $2\theta = 35.5°$ correspond to the (220), (400) and (311) planes of Fe_3O_4. It indicates that there is a small amount of Fe_3O_4 phase

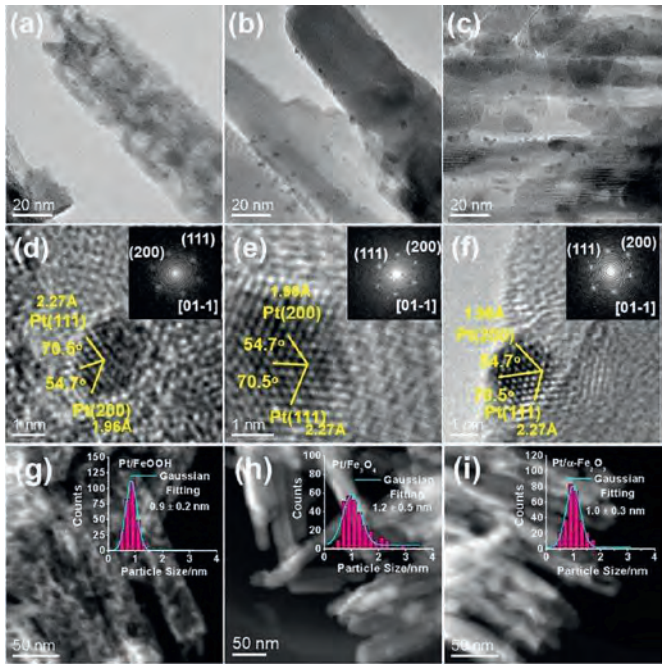

Fig. 2. Low-magnification TEM (a–c), HRTEM (d–f) and HAADF-STEM (g-i) images of Pt/FeOOH (a, d, g), Pt/Fe_3O_4 (b, e, h) and Pt/α-Fe_2O_3 (c, f, i) catalysts. The insets in d-f and g–i are the corresponding local FFTs and PSD histograms, respectively.

in FeOOH support due to the phase transition in catalyst synthesis process, but it has not been found in HRTEM characterization Fig. S6 in Supporting information. There is no change in crystal structure for Fe_3O_4 and α-Fe_2O_3 supports in Pt/Fe_3O_4 and Pt/α-Fe_2O_3 catalysts (Fig. 1 and Fig. S6). Moreover, there is no obvious peaks of Pt NPs are found in these three catalysts, indicating the significantly small sizes of Pt NPs on the supports. TEM images (Figs. 2a-c) clearly show that Pt NPs are uniformly deposited on different supports. Statistical analysis of particle size distribution (PSD) was carried out by randomly measured ca. 300 Pt NPs (the insets in Figs. 2g–i). For Pt/FeOOH, Pt/Fe_3O_4 and Pt/α-Fe_2O_3 catalysts, the PSD histograms present the average size of Pt NPs are 0.9, 1.2 and 1.0 nm, respectively. It reveals that the particle sizes of Pt NPs are slightly related to the properties of supports. A more detailed analysis on PSD indicates that Pt NPs on Pt/FeOOH exhibited a narrower range with 0.3–1.7 nm. The outstanding dispersion of Pt NPs on FeOOH support may be ascribed to its highest surface area arising from the mesoporous structure. The HRTEM images of Pt NPs are shown in Figs. 2d–f. The measured lattice spacings of 2.27 Å and 1.96 Å, obtained by forming an angle of 54.7° for the Pt nanocrystals, corresponding to the face-centered cubic (fcc) Pt (111) and (200) planes. The ambiguous isolated diffraction spots in fast Fourier transform (FFT) patterns (the insets in Figs. 2d-f) also displays the crystal structure of Pt NPs. Moreover, it can be seen that the Pt NPs immobilized on the three supports possess the same FFT patterns, indicating the supports have no effect on the crystal structure of Pt NPs. Furthermore, scanning electron microscopy (SEM) and annular dark-field STEM (ADF-STEM) images of Pt/FeOOH catalysts (Fig. 3) shown that Pt NPs are mainly anchored at the pore edge of FeOOH support (marked by white circles), which may improve the dispersion of Pt NPs.

XPS was used to unravel the surface chemical states and elemental composition of the catalysts. The O 1s spectra of the series Pt-based samples (Fig. 4a) were deconvoluted into two components, including the lattice oxygen (O_a) and surface hydroxyl species (O_b) [26]. The ratios of O_b/O_a were 0.63, 0.39 and 0.43 for Pt/FeOOH, Pt/Fe_3O_4 and Pt/α-Fe_2O_3, respectively. It is clearly that

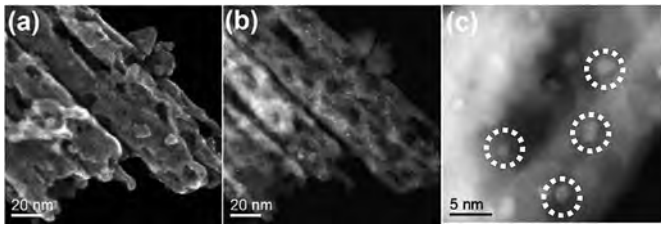

Fig. 3. SEM (a) and ADF-STEM (b, c) images of Pt/FeOOH catalyst.

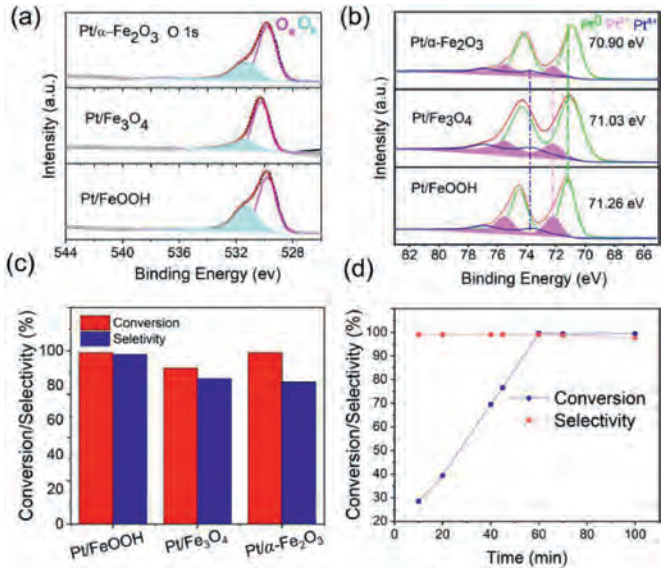

Fig. 4. O 1s (a) and Pt 4f (b) XPS spectra of Pt/FeOOH, Pt/Fe_3O_4 and Pt/α-Fe_2O_3 catalysts. Catalytic performance of Pt/FeOOH, Pt/Fe_3O_4 and Pt/α-Fe_2O_3 catalysts in 3-NS hydrogenation reaction (c). (reaction conditions: T = 45 °C, P = 5 bar, 20 mg catalysts, 10 mL toluene was used as solvent, reaction time: 70 min). The conversion and selectivity over Pt/FeOOH catalyst with different reaction time (d).

Table 1
The surface element composition of Pt/FeOOH, Pt/Fe_3O_4 and Pt/α-Fe_2O_3 catalysts.

Sample	Surface element composition			
	O_b/O_a	Pt^0	Pt^{2+}	Pt^{4+}
Pt/FeOOH	0.63	71.1	21.4	7.5
Pt/Fe_3O_4	0.39	76.6	14.0	9.4
Pt/α-Fe_2O_3	0.43	81.6	13.8	4.6

the surface hydroxyl groups in Pt/FeOOH is much higher than other samples. The XPS spectra of Pt 4f are depicted in Fig. 4b. Pt 4f spectra could be deconvoluted into three components for all catalysts, including the metallic Pt^0, Pt^{2+} and Pt^{4+} [24]. The existence of Pt^{4+} may be caused by the weak reduction capability of EG. Apparently, the supports have a crucial effect on Pt 4f binding energy. An appreciable shift to higher values of Pt^0 binding energy is observed for Pt/FeOOH. A quantitative analysis of Pt components was obtained from the area of the corresponding fitting Gaussian peaks after nonlinear Shirley-type background subtraction and summarized in Table 1.

Pt/FeOOH sample shows the lowest content of Pt^0 and the highest content of oxide state Pt. It was deduced that the electronic structure of Pt was adjusted by surface hydroxyl groups in FeOOH [27,28] and there may exist more electron transfer from Pt to FeOOH support. The difference of Pt^0 concentration between Pt/Fe_3O_4 and Pt/α-Fe_2O_3 may be caused by the surface oxygen species [29].

The hydrogenation of 3-NS can produce 3-AS and 3-ethylnitrobenzene (ENB) by hydrogenation of nitro and vinyl group, respectively, and then produce 3-ethylaniline (3-EA) *via* the complete hydrogenation of both the nitro and vinyl groups. In a series of blank tests, the reactions carried out with the support alone did not result in any measurable conversion. The catalytic performance of the series Pt-based catalysts for 3-NS hydrogenation is shown in Fig. 4c. Pt/FeOOH catalyst exhibits the best catalytic performance with 98% selectivity to 3-AS at a 99% 3-NS conversion after 70 min of reaction. The catalytic activity over Pt/FeOOH catalyst was also studied in 3-NS hydrogenation with the extension of reaction time. The conversion of 3-NS increases with reaction time and reaches closely to 100% at 60 min as shown in Fig. 4d. As the reaction time is prolonged, the conversion of 3-NS is maintained and the selectivity to 3-AS does not change significantly. In contrast, for Pt/Fe_3O_4 and Pt/α-Fe_2O_3, the selectivity to 3-AS was only 84% and 82% after 70 min of reaction, respectively, which are lower than that of Pt/FeOOH. A comparison of the catalytic performance with some representative reported catalysts for the 3-NS hydrogenation indicates that Pt/FeOOH catalysts in this work show significant advantages [4,5,30]. It has been illustrated that Pt species with positive charges are favorable to the adsorption of the nitro group [11], which may contribute to the excellent catalytic performance of Pt/FeOOH. Pt/FeOOH catalyst was chosen for stability test because of its excellent activity and selectivity. The result is presented in Fig. S7 (Supporting information), which showed that the conversion of 3-NS remained at 99.7% and the selectivity to 3-AS is slightly decreased from 95.1% to 91.7% after the forth runs. It indicates that Pt/FeOOH catalyst has good stability and can be reused.

Platinum NPs supported on a series of iron compounds (FeOOH, Fe_3O_4 and α-Fe_2O_3) were synthesized and their catalytic performance were tested in the chemoselective hydrogenation of 3-NS. Among these catalysts, Pt/FeOOH exhibited excellent selectivity toward the target product of 3-AS (98%) at 99% 3-NS conversion. It was found that there are more -OH group on the surface of FeOOH, which changed the electronic structure of the supported Pt NPs. The excellent catalytic performance of Pt/FeOOH could be attributed to the positively charged Pt species, which is intrinsically more selective for -NO_2 hydrogenation than for vinyl hydrogenation. In this work, we design a promising strategy for engineering the electronic properties of Pt by exploring the interaction between noble metal NPs and -OH functional groups on the support surface. This will provide some guidelines for synthesizing other supported metal catalysts with superior catalytic performance.

Declaration of competing interest

The authors declare no conflicts of interests.

Acknowledgments

The authors gratefully acknowledge the financial support provided by the National Natural Science Foundation of China (Nos. 22072164, 21773269, 51932005 and 21761132025) and the Liao Ning Revitalization Talents Program (No. XLYC1807175). The authors thank to Mr. Hiroaki Matsumoto (Hitachi High-Technologies Co., Ltd.) for the SEM and STEM images in Fig. 3.

Supplementary materials

Supplementary material associated with this article can be found, in the online version, at doi:10.1016/j.cclet.2021.10.049.

References

[1] M.Q. Shen, H. Liu, C. Yu, et al., J. Am. Chem. Soc. 140 (2018) 16460–16463.
[2] X.R. Wei, M.Y. Zhou, X.C. Zhang, X.N. Wang, Z.X. Wu, ACS Appl. Mater. Interfaces 11 (2019) 39116–39124.
[3] W.L. Wu, S.T. Zhao, Y. Cui, et al., ChemCatChem 11 (2019) 2793–2798.
[4] T.T. Gao, W. Shi, Y. Zhang, et al., Chem. Eur. J. 26 (2020) 8990–8996.

[5] M.L. Lan, B. Zhang, H.Y. Cheng, et al., Mol. Catal. 432 (2017) 23–30.
[6] M. Macion, A.J. Barnes, S.M. Althahban, et al., Nat. Catal. 2 (2019) 873–881.
[7] X.Q. Xie, Z.J. Wu, N. Zhang, Chin. Chem. Lett. 31 (2020) 1014–1017.
[8] Y. Tan, X.Y. Liu, L.L. Kang, A.Q. Wang, T. Zhang, J. Catal. 364 (2018) 174–182.
[9] S. Ken-ichi, M. Yuji, S. Atsushi, J. Catal. 270 (2010) 86–94.
[10] P. Serna, P. Concepción, A. Corma, J. Catal. 265 (2009) 19–25.
[11] H.S. Wei, X.Y. Liu, A.Q. Wang, et al., Nat. Commun. 5 (2014) 5634.
[12] G. Vilé, N. Almora-Barrios, N. López, J.P. Ramírez, ACS Catal. 5 (2015) 3767–3778.
[13] A. Corma, P. Serna, P. Concepción, J.J. Calvion, J. Am. Chem. Soc. 130 (2008) 8748–8753.
[14] H.S. Wei, Y.J. Ren, A.Q. Wang, et al., Chem. Sci. 8 (2017) 5126–5131.
[15] A. Shukla, R.K. Singha, T. Sasaki, R. Bal, Green Chem. 17 (2015) 785–790.
[16] T.W. van Deelen, C.H. Mejía, K.P. de Jong, Nat. Catal. 2 (2019) 955–970.
[17] J. Zhang, L. Wang, Z.Y. Wu, et al., Acta Phys. Chim. Sin. 36 (2020) 1912001.
[18] Y. Lou, J. Xu, H.L. Wu, J.Y. Liu, Chem. Commun. 54 (2018) 13248–13251.
[19] W. Shi, T.T. Gao, L.Y. Zhang, et al., Chin. J. Catal. 40 (2019) 1884–1894.
[20] J.S. Chen, J.J. Ding, H.Q. Li, et al., Catal. Sci. Technol. 9 (2019) 3287–3294.
[21] C. Evangelisti, L.A. Aronica, M. Botavina, et al., J. Mole. Catal. A: Chem. 366 (2013) 288–293.
[22] L.Q. Liu, F. Zhou, L.G. Wang, et al., J. Catal. 274 (2010) 1–10.
[23] B. Zheng, G. Liu, L.L. Geng, et al., Catal. Sci. Technol. 6 (2016) 1546–1554.
[24] W. Shi, B.S. Zhang, Y.M. Lin, et al., ACS Catal. 6 (2016) 7844–7854.
[25] B.Z. Fang, N.K. Chaudhari, M.S. Kim, J.H. Kim, J.S. Yu, J. Am. Chem. Soc. 131 (2009) 15330–15338.
[26] J.C. Dupin, D. Gonbeau, P. Vinatier, A. Levasseur, Phys. Chem. Chem. Phys. 2 (2000) 1319–1324.
[27] Y.P. Zhai, D. Pierre, R. Si, et al., Science 329 (2010) 1633–1636.
[28] R. Subbaraman, D. Tripkovic, D. Strmcnik, et al., Science 334 (2011) 1256–1260.
[29] M. Yang, J.J. Liu, S. Lee, et al., J. Am. Chem. Soc. 137 (2015) 3470–3473.
[30] Q.F. Wu, C. Zhang, W.W. Lin, et al., Catalysts 9 (2019) 428.